Pergamon

J. Aerosol Sci. Vol. 30, No. 8, pp. 983–999, 1999

Printed in Great Britain
PII: S0021-8502(98)00767-8
0021-8502/99/$ - see front matter

DESIGN AND TESTING OF AN AEROSOL/SHEATH INLET FOR HIGH RESOLUTION MEASUREMENTS WITH A DMA

Da-Ren Chen,* David Y. H. Pui,*† George W. Mulholland‡ and Marco Fernandez‡

* Particle Technology Laboratory, Mechanical Engineering Department, University of Minnesota, 111 Church Street, S.E. Minneapolis, MN 55455, U.S.A.
‡ National Institute of Standards and Technology, Gaithersburg, MD 20899, U.S.A.

(*First received* 10 *October* 1997; *and in final form* 5 *October* 1998)

Abstract—A modified aerosol/sheath inlet was designed for a differential mobility analyzer (DMA) for high resolution measurements based on field model calculations which include fluid flow, electric field, and convective/diffusive transport. To avoid the predicted flow recirculation for the current inlet design at an aerosol-to-sheath flow ratio of 0.05, the slit width is reduced and aerodynamically shaped so that the sheath velocity and aerosol velocity more nearly match. Numerical results are presented comparing the fluid flow of the old and new inlet. Problems associated with the old inlet include: flow unsteadiness at a flow ratio of 0.025, voltage shift at the peak particle concentration as a function of the flow ratio, and the historical observation that, while performing tandem differential mobility analyzer measurements (TDMA), the voltage applied on the second DMA for the peak particle concentration is higher than that for the first. Measurements demonstrate that all these problems are reduced or eliminated with the new inlet design. The TDMA measurements include flow ratios of 0.1, 0.05, 0.025 and 0.0125 at sheath flows of 166 and 333 $cm^3 s^{-1}$ (10 and 20 l min^{-1}). The challenge of performing measurements at these low flow ratios will be discussed including flow calibration, flow matching, and pressure monitoring. The new inlet is applied to the measurement of the National Institute of Standards and Technology 0.1 μm Standard Reference Material 1963, and it is shown that the DMA can accurately measure the standard deviation of this narrowly distributed aerosol ($\sigma/D_p = 0.02$).

INTRODUCTION

The development of a differential mobility analyzer (DMA) optimized for high resolution measurements is important for characterizing the size distributions of narrowly distributed calibration standards. Such standards are needed covering the size range from 50 nm to at least 500 nm in the semiconductor manufacturing field. These standards are needed for the calibration of scanning surface inspection systems, which are used for detecting particles on silicon wafers (Mulholland *et al.*, 1996). The National Technology Roadmap for Semiconductors (NTRS) discusses particles as small as 60 nm in diameter being a concern by the year 2001. It is important that the calibration standards be monosized with coefficient of variation, σ/D_p, less than 0.05, because the inspection systems are based on scattered light. The scattering intensity for the smallest particles on a surface varies as the particle diameter raised to the sixth or larger power so that a small change in diameter produces a relatively large change in the instrument output. For example, a 12% increase in particle size produces a doubling in the total scattering signal. The high resolution DMA can also be used to classify nanometer particles required for advanced technological applications because of their enhanced mechanical, optical, or electrical/magnetic properties. These applications often require monosize particles, $\sigma/D_p < 0.05$, which can be accomplished using the high resolution DMA described in this study.

The most widely used method for determining the size distribution of nearly monosize particles, such as polystyrene spheres, is electron microscopy. The disadvantages of this method are that it is slow and labor intensive in terms of sample preparation and measurement even though the development of image analysis software has reduced the time required for particle analysis. There is a need for rapid size distribution measurements for not only accurate sizing of particle standards but also for process monitoring to improve

†Author to whom correspondence should be addressed.

synthesis methods for monosize particles. The DMA in combination with a condensation particle counter has the ability to process hundreds of particles per second and to measuring a size distribution with 10 size increments in less than 5 min. Because of the high number of particles counted, the sample statistics are not an issue as is the case for electron microscopy studies, where typically only 100–300 particles are sized.

While the operation of the DMA is ideal in terms of throughput, there has been relatively few published studies regarding the performance of the classifier for high resolution measurements for $\sigma/D_p < 0.05$ or σ_g less than 1.03 beyond the original study by Knutson and Whitby (1975) involving an analysis of moments. Mulholland *et al.* (1996) used a low flow ratio of 0.025 to measure the widths of the size distributions of 23 polystyrene samples with mean sizes in the range 70–300 nm. The ratios of half-width at half-height (HWHH) to the mean size were found to be in the range 0.015–0.08. These values provided the correct trend but were overestimates of the true width of the size distribution because of instrumental broadening. There are needs both in terms of hardware and software for improving the DMA for use in accurate size distribution measurements for narrowly distributed aerosols. Current software focuses on broader size distribution where the DMA sizing resolution is much finer that the width of the size distribution. Whereas, for monosize particles ($\sigma/D_p < 0.03$), the size distribution width and the DMA size resolution, which is approximately equal to 1/2 the flow ratio, are similar in size. In addition there is a need to change the inlet of the DMA to overcome limitations of the current design for high resolution measurements as discussed below. The design, fabrication, and testing of the modified inlet is the principle focus of this paper.

PROBLEMS ASSOCIATED WITH CURRENT TSI DMA INLET DESIGN

The DMA is illustrated in Fig. 1 including the inlet flow region, the central electrode, and the exit flow region. The charged aerosol particles are deflected by the electric field, and those particles having electrical mobilities within a narrow band will exit through the slit in the central electrode. As shown originally by Knutson and Whitby (1975), the size resolution of the DMA is proportional to the aerosol/sheath flow ratio in the classifying region. So the DMAs have a good potential for high resolution measurement by operating at a small flow ratio. The resolution of the current TSI DMA,* however, is less than predicted for an aerosol/sheath flow ratio of 0.05 with a maximum sheath flow of 333 $cm^3 s^{-1}$ (20 l min^{-1}). As revealed in the numerical model of the DMA by Chen and Pui (1997), the mismatch of aerosol and sheath flow velocities at the wide inlet slit of the TSI DMA is the major cause of this limitation. Figure 2 shows the flow pattern at the region near the entrance slit (see Fig. 1 for location of entrance slit) for two aerosol/sheath flow ratios (a) 1/10 (l min^{-1})/(l min^{-1}) and (b) 1/20 (l min^{-1})/(l min^{-1}). As shown in the figure, flow recirculation zones were predicted in both cases. The area of the recirculation zone increases with decreasing aerosol/sheath flow ratio. For the case of 1/20 ratios, the area covers approximately 50% of the entire entrance slit. It is anticipated that the situation will deteriorate even more when using lower aerosol/sheath flow ratio.

The recirculation problems are likely responsible for the following three observations. First, it is difficult to maintain flow steadiness at low flow ratios. When the recirculation zone has a small area and is confined to the corner, the flow pattern is expected to be steady. However, when the recirculation grows large enough to block out a significant portion of the inlet passage, the flow pattern will become very sensitive to flow fluctuation which is commonly seen in flow control processes. Unfortunately, this is the case at 1/20 (l min^{-1})/(l min^{-1}) aerosol/sheath flow ratio. As a consequence, the flow in the DMA classification region is unstable, and it limits the TSI DMA operating range to a higher aerosol/sheath

* Certain materials and equipment are identified in this paper in order to adequately specify the experimental procedure. Such identification does not imply recommendation or endorsement by the National Institute of Standards and Technology, nor does it imply that the materials or equipment are necessarily the best available for the purpose.

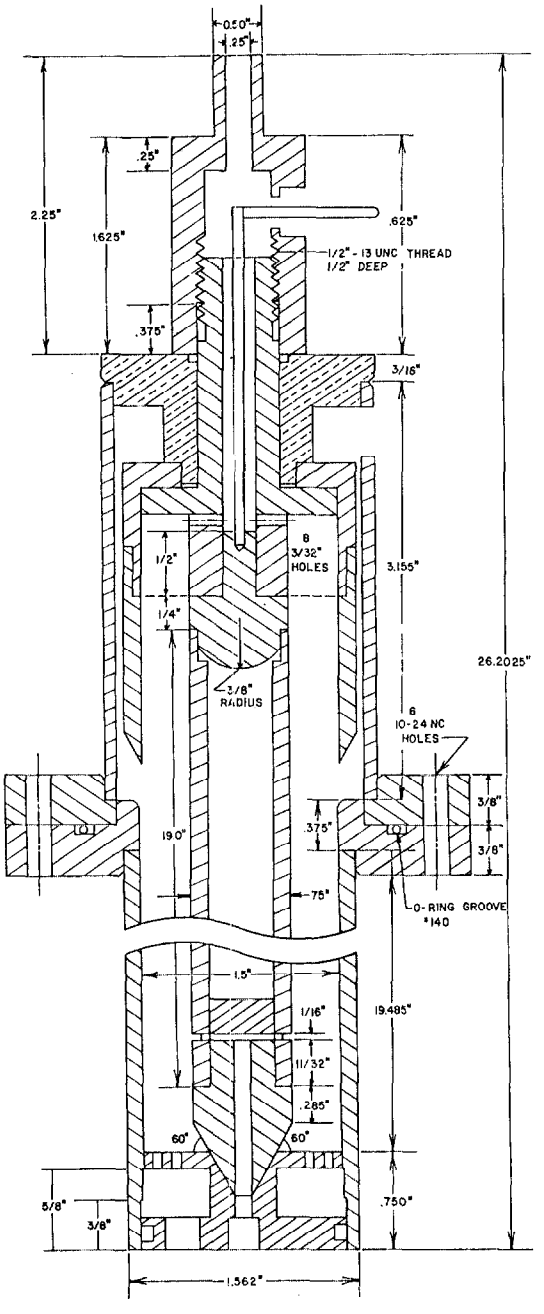

Fig. 1. Schematic diagram of the UM-TSI Differential Mobility Analyzer (Liu and Pui, 1974).

flow ratio (lower resolution). To illustrate this problem, Fig. 3 shows the scans of 0.1 μm NIST Standard Reference Material (SRM) particles at (a) 1/10 and (b) 0.25/10 aerosol/sheath flow ratios. Two scans are included for each flow ratio. The first scan is obtained by increasing the applied voltage on the DMA collector tube (up-scan) from the lowest setting and the second by decreasing the applied voltage (down-scan) from the highest setting. For the 1/10 flow ratio, the two scans are almost identical. However, significantly different scans are obtained for the 0.25/10 flow ratio. This hysterisis is often observed when the TSI DMA is operated at low aerosol/sheath flow ratios.

The second problem is an observed voltage shift of the peak particle concentration for different aerosol/sheath flow ratios. This phenomenon had been documented in the paper of Kinney *et al.* (1991). In their work, 0.269 μm NIST SRM PSL spheres were measured. The

DMA voltage required to obtain the peak particle concentration increased when the flow ratio changed from 2.5/10 to 0.5/10. A similar voltage shift was observed for 0.1 μm NIST SRM particles when different flow ratios were used. The reason for the shifts was not explained in that paper. The same effect has also been observed in tandem-DMA (TDMA) experiments. Figure 4 shows TDMA scans for different aerosol flow rates for a fixed sheath air flow rate of 333 $cm^3 s^{-1}$ (20 l min^{-1}). The electrical mobility on the abscissa was normalized with the central mobility, Z_p^*, of 5.33×10^{-4} $cm^2 V^{-1} s^{-1}$, which is determined by the first DMA. The normalized electrical mobility for peak concentration is seen to decrease with decreasing aerosol/sheath flow ratio. When one considers the numerical results of flow recirculation (Fig. 2), a plausible explanation for the voltage shift becomes clear. Reducing the aerosol flow rate while keeping the sheath flow rate constant enlarges the recirculation zone, which moves the aerosol/sheath flow matching position towards the upper portion of the wide entrance slit. This increases the active length of the central electrode which is defined as the distance between the aerosol exit point from the entrance slit and the mid-point of the aerosol exit slit near the bottom of the collector tube. The increase in the effective length can be as much as 1%. The applied voltage for the peak particle concentration will be shifted to a higher voltage.

The third problem is the historical observation that, while performing TDMA experiments, the voltage applied to the second DMA to obtain the peak particle concentration has always been higher than that applied to the first DMA. This observation has been reported in many papers, e.g. Rader and McMurry (1986), and Kousaka *et al.* (1986). We have observed the same effect as illustrated in Fig. 4. For the aerosol flow rates studied, the normalized electric mobility corresponding to the peak concentration is always less than unity, i.e. a higher voltage is required on the second DMA to obtain the maximum particle concentration. This phenomenon has been attributed to the effects of Brownian diffusion and space charge (Alonso and Kousaka, 1996; Camata *et al.*, 1996). These effects, however, cannot explain all cases. For example, in the experiment of Rader and McMurry (1986), the aerosol concentration was typically below 10^5 particles cm^{-3} (too low a concentration to produce a significant space charge effect) and the particle size range was from 0.010 μm to 0.2 μm (a sufficiently large size to minimize diffusional effects).

We have used our numerical model to examine the flow recirculation and electric field around the entrance slit. We believe that the voltage shift is caused by the increased electric field needed to draw out the particles trapped in the flow recirculation zone. Figure 5 shows the calculated electric potential lines around the slit region. The electric potential field lines are seen to penetrate deep into the slit opening which includes much of the recirculation zone. It is plausible that when the voltage is applied on the collection rod of the first DMA, particles with lower electrical mobility will not be trapped in the re-circulation zone. Thus, the particle concentration peaks at a higher voltage when the classified particles are passed through the second DMA.

The objective of this study is to design a new inlet that eliminates or minimizes the above-stated problems. Experiments are performed to examine the hypotheses described above and to obtain the performance of the new inlet design.

NEW INLET DESIGN

A proposed approach to avoiding flow recirculation at the aerosol inlet slit is to reduce the slit width, to confine the flow by filling the open zone, and to aerodynamically shape the inlet. Figure 6 shows a new inlet incorporating these ideas. The new inlet is designed so that the existing TSI DMAs can be retrofitted easily by inserting a ring machined with the required modifications. The ring is machined to rest on the bottom shoulder of the existing entrance slit. Detailed dimensions are given in the figure. A 45° sloped wall is used to guide the aerosol gradually into the classifying region. Following a similar approach used successfully in the inlet design of the Nano-DMA (Chen *et al.*, 1998), the slit width is reduced in order to improve flow velocity matching in the classifying region and to avoid electric field penetration into the upstream side of the entrance slit.

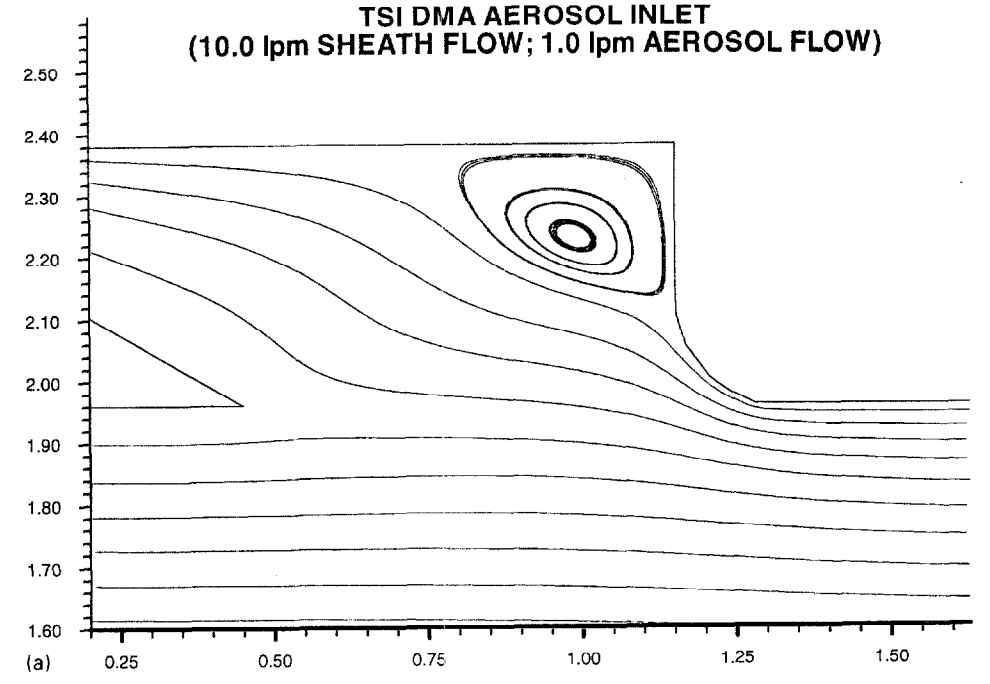

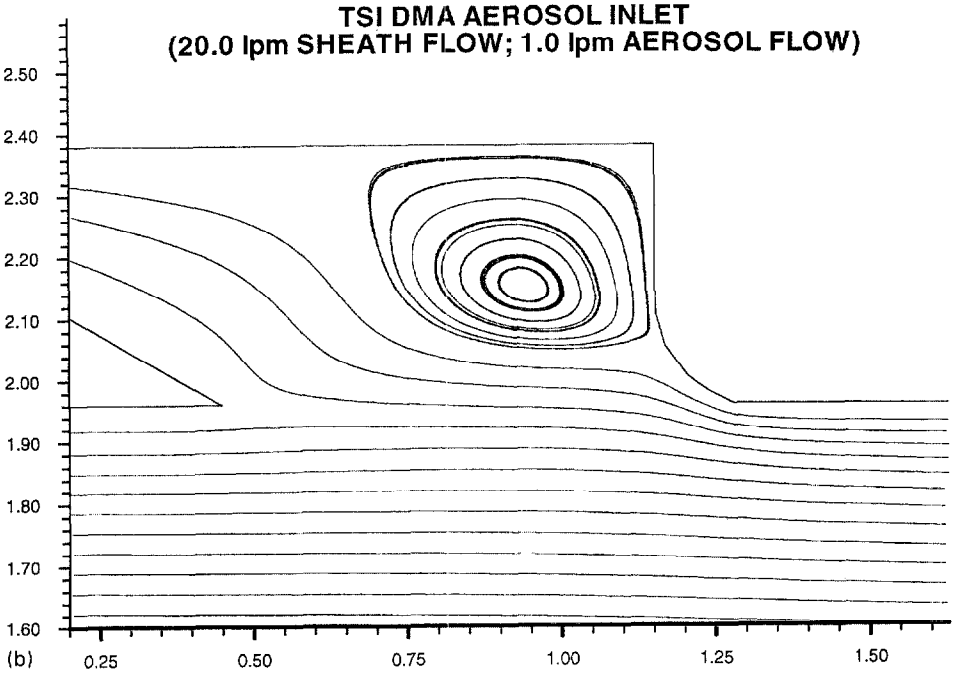

Fig. 2. Flow pattern for the region close to the aerosol entrance slit of TSI DMA at (a) 1.0/10 (b) 1.0/20 aerosol/sheath flow ratios.

Fabrication of inlet

The ring assembly was machined from stainless steel to the same tolerance as the original DMA. The biggest challenge was to measure the actual gap spacing between the ring insert and the existing conical inlet. When the system is assembled, the gap is not visible so an

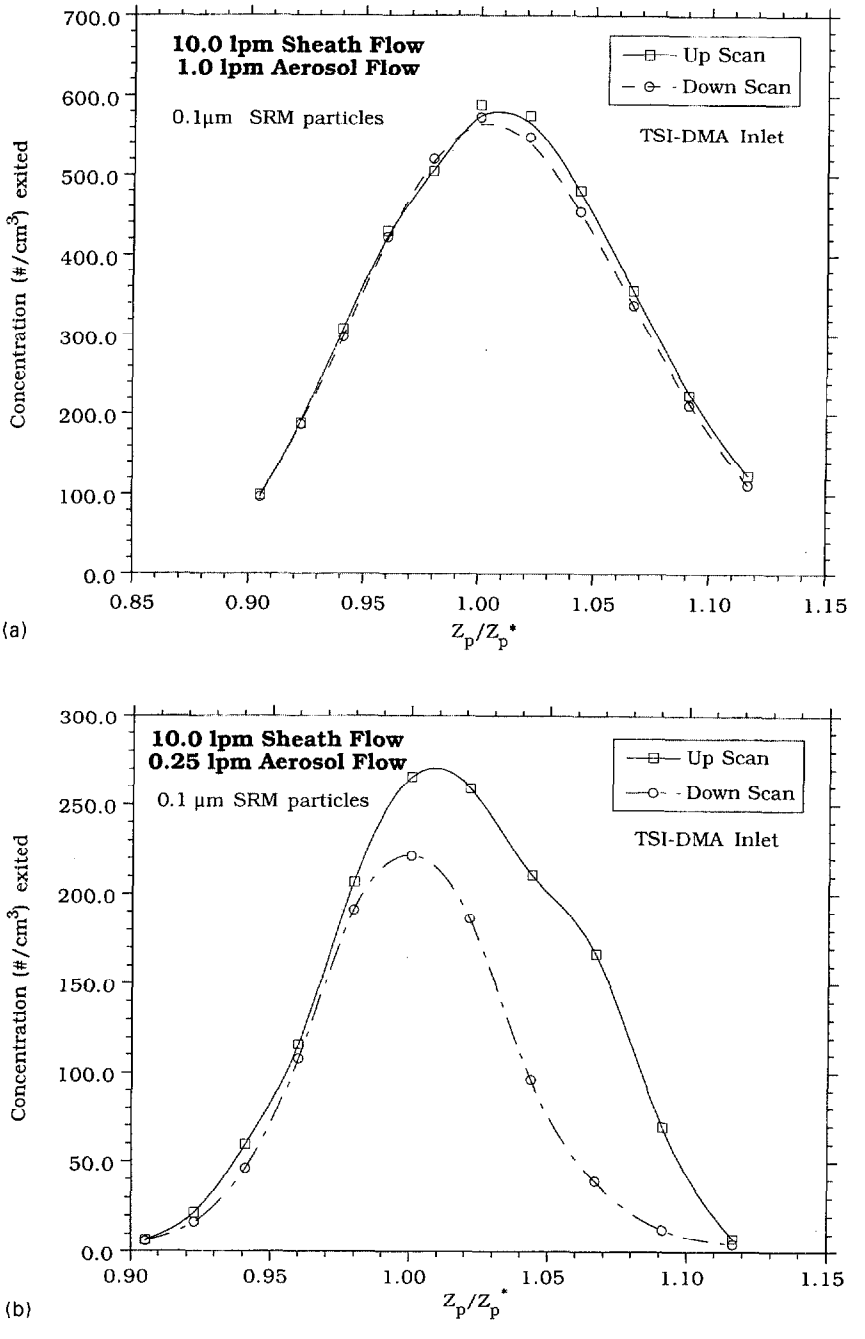

Fig. 3. TSI DMA scans of 0.1 μm SRM particles at the flow ratios of (a) 1/10 and (b) 0.25/10.

indirect method of sizing the gap was needed. The method used was adopted from the "imprint" technology used by dentists. Vinyl polysiloxane impression material (Reprosil) was used to make the imprint. Material from the catalyst tub and the base tub are quickly mixed and a pliable ring is formed around the inlet ring. The ring is then inserted in the DMA with the pliable material providing an imprint of the gap between the ring and the conical inlet. The impression material is allowed to set up for 15 min, the ring assembly is disassembled, and the impression material removed. The material is sectioned into several thin pieces around the circumference so that the gap can be measured. The gap was found to vary from 0.75 to 0.78 mm around the circumference of the ring. The original gap was approximately 9 mm.

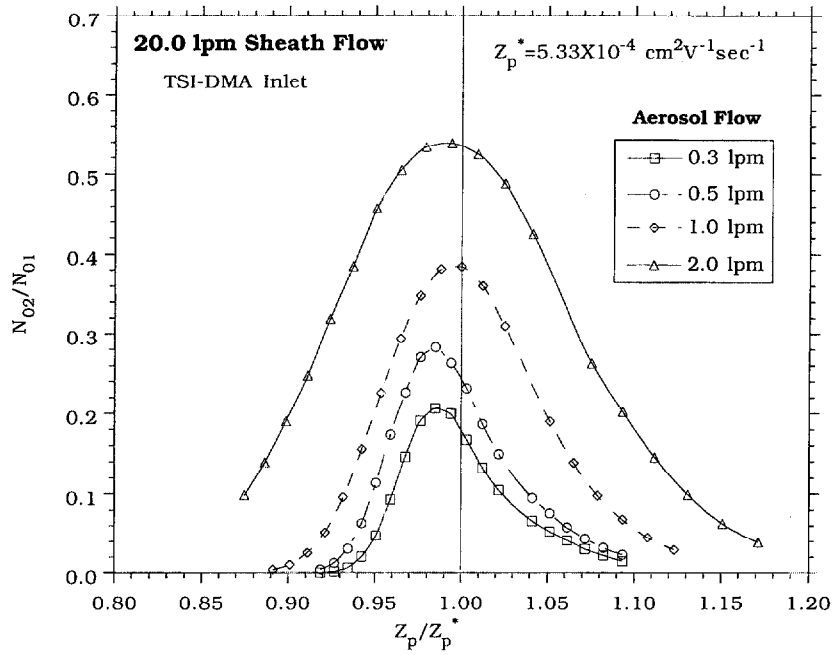

Fig. 4. TDMA scans of particles with Z_p^* of $5.33 \times 10^{-4}\,\mathrm{cm^2\,V^{-1}\,s^{-1}}$ at different aerosol/sheath flow ratios (The sheath flow is fixed at $333\,\mathrm{cm^3\,s^{-1}}$ ($20\,\mathrm{l\,min^{-1}}$).

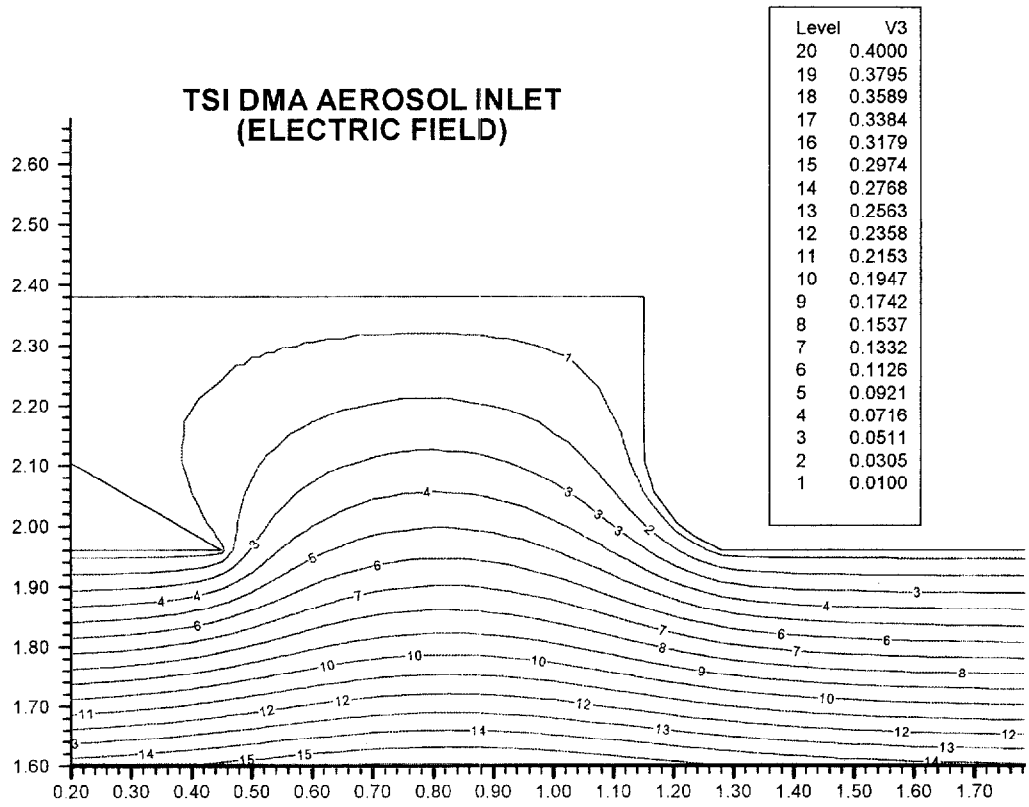

Fig. 5. Electric equipotential lines around the region close to the aerosol entrance slit of the TSI DMA. (V3: dimensionless voltage 0–1 indicated by level χ)

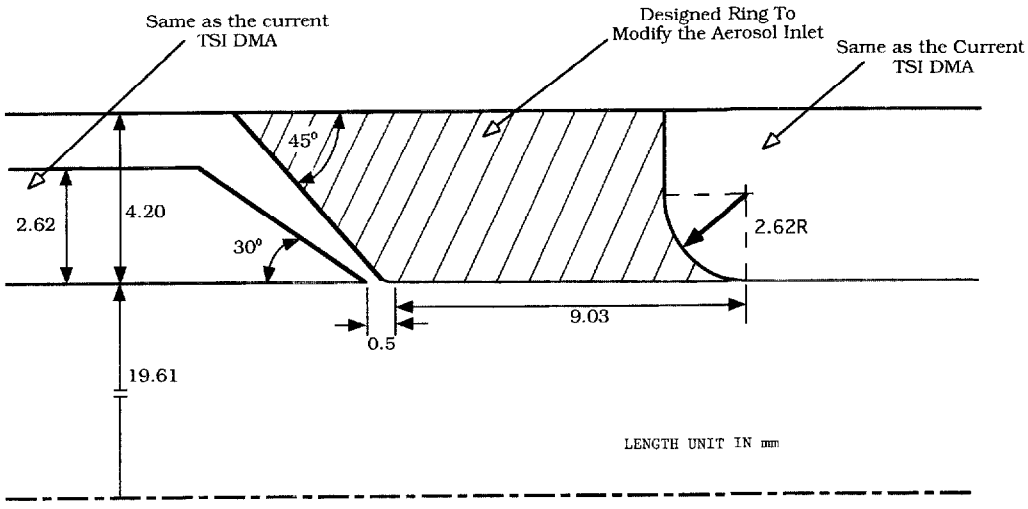

Fig. 6. Drawing of the modified aerosol inlet slit.

Numerical approach

Prior to the construction of the inlet ring, the performance of the TSI DMA with this modified inlet was evaluated using the numerical model developed by Chen and Pui (1997). The computational domain consists of the aerosol transport passage starting from the exit of the aerosol plenum chamber and extending through the classifying region of the TSI DMA. The exit aerosol transport passage is not included. Figure 7 shows the mesh distribution around the region where the aerosol flow and the sheath flow meet. Finer meshes are distributed in the regions requiring close examination and the regions where high velocity gradients are encountered, e.g. near the walls.

Flow matching at various flow ratios up to 1/100. The streamlines at aerosol/sheath flow ratios of 0.2/20, 0.5/20, 1/20, and 2/20 are shown in Fig. 8. For all the flow ratios tested, the aerosol flow enters smoothly into the classifying region without recirculation. The flow ratios evaluated cover a range of 0.01–0.1. For the case of a 0.2/20 ratio, the spacings between the sheath air flow streamlines in the region where the aerosol flow first meets the sheath flow are quite large. Since the same volume flow passes between two adjacent stream lines, this indicates that the flow shear stress there is quite small. However, the spacings are reduced as the aerosol flow rate is increased, indicating that the flow shear stress is becoming larger with increasing aerosol flow velocity. Since flow instability is likely to occur in regions of high shear stress, the highest aerosol flow rate of 33.3 $cm^3 s^{-1}$ (2 l min^{-1}) may be at or approaching a flow instability condition.

Electric field. Figure 9 shows electric equipotential lines in the vicinity of the modified aerosol inlet. Due to the narrow slit width, electric field penetration into the aerosol transport passage is significantly reduced compared with that shown in Fig. 5.

Numerical transfer functions. Transfer functions for different aerosol flow ratios were calculated based on a broad initial aerosol size distribution going through two DMAs in series with identical settings. Figure 10 shows the transfer functions of classifying particles with a central mobility, Z_p^*, of 5.33×10^{-4} $cm^2 V^{-1} s^{-1}$, at aerosol flow rates of 5, 8.3, 16.6, and 33.3 $cm^3 s^{-1}$ (0.3, 0.5, 1, and 2 l min^{-1}), and a fixed sheath air flow rate of 333 $cm^3 s^{-1}$ (20 l min^{-1}). The stated electrical mobility corresponds to a singly charged particle with diameter of 67.0 nm. As seen in the figure, the height of the transfer function decreases with decreasing aerosol flow rate. This effect is expected because reducing the aerosol flow rate

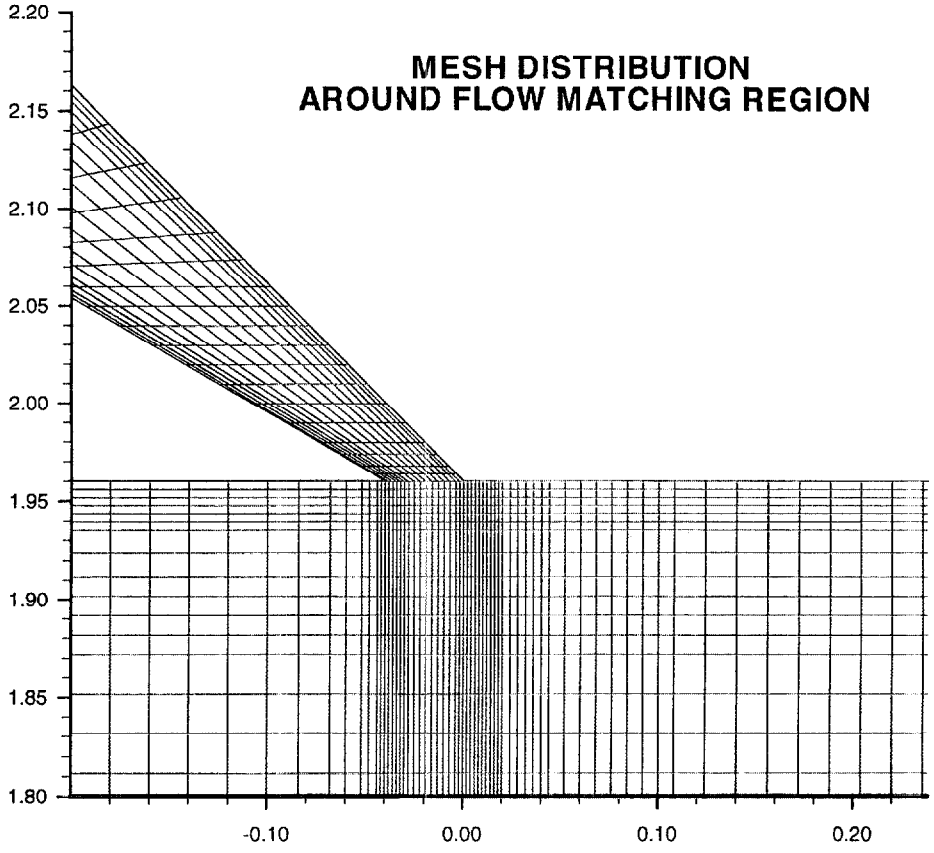

Fig. 7. Mesh distribution around the region close to the modified aerosol entrance slit.

will increase the aerosol residence time in the aerosol inlet region and consequently increase the particle loss due to Brownian motion. Meanwhile, the full-width at half-peak-height (FWHP) decreases as the aerosol flow decreases. It should be noted that, when the aerosol s^{-1}heath flow ratio is reduced significantly more, the decrease in the FWHP is limited due to Brownian motion.

Figure 11 shows the transfer functions for particles with the central mobility of 2.69×10^{-4} $cm^2 V^{-1} s^{-1}$ and aerosol flow rates of 4.2, 8.3, and 16.6 $cm^3 s^{-1}$ (0.25, 0.5 and 1 l min^{-1}). For this calculation, the sheath air flow rate is kept constant at 166 $cm^3 s^{-1}$ (10 l min^{-1}). The electrical mobility corresponds to a particle diameter of 98.3 nm. The observed trends in this case are similar to those described above.

Experimental evaluation

Experimental setup and procedure. The measurement procedure is nominally similar to other experiments using tandem differential mobility analyzers, e.g. Rader and McMurry (1986). Major considerations in the experimental design include matching the sheath and excess flow in the first DMA and measuring the flows in the second DMA relative to the first. Two different aerosols were generated. The first was produced by nebulizing a solution of 0.4% by mass NaCl diluted by clean water (18 megaohm deionized water filtered with a 0.2 μm pore size filter) using a TSI 3075 atomizer at a gauge pressure of 207 kPa (30 psig). A 1 l reservoir allowed operation for about 8 h in a recirculating mode with steady output before replacement of the solution. NIST SRM 1963, which is a 0.5% by mass suspension of monosize 0.1 μm polystyrene spheres in water, was used in generating the second aerosol. One drop of the SRM was diluted with 200 ml of clean water before nebulizing. In this case

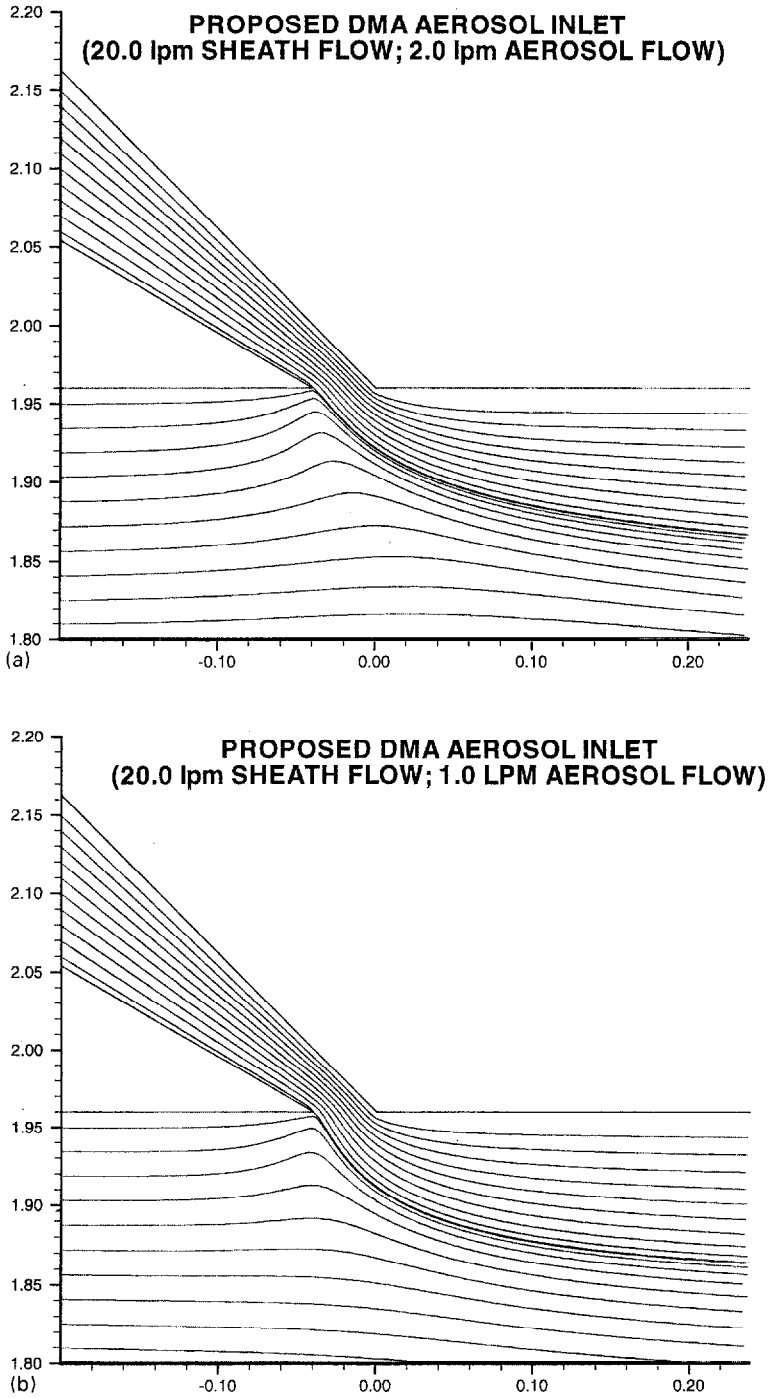

Fig. 8(a) and (b). Flow matching conditions at (a) 33.3 $cm^3 s^{-1}$ (2.0 l min^{-1}) and (b) 16.6 $cm^3 s^{-1}$ (1 l min^{-1}), aerosol flow rates when the proposed aerosol entrance slit is installed (The sheath flow is kept constant at 333 $cm^3 s^{-1}$ (20.0 l min^{-1})).

the JSR Aeromaster-1 was used for producing the aerosol. Key features of this nebulizer include temperature controlled capillary feed, a heated tube for evaporating water droplets rather than using desiccant, and no recirculation of the liquid feed.

An illustration of the apparatus is given in Fig. 12. The water evaporated as the aerosol flowed at 83 $cm^3 s^{-1}$ (5 l min^{-1}) through a diffusion drier and was mixed with 167 $cm^3 s^{-1}$

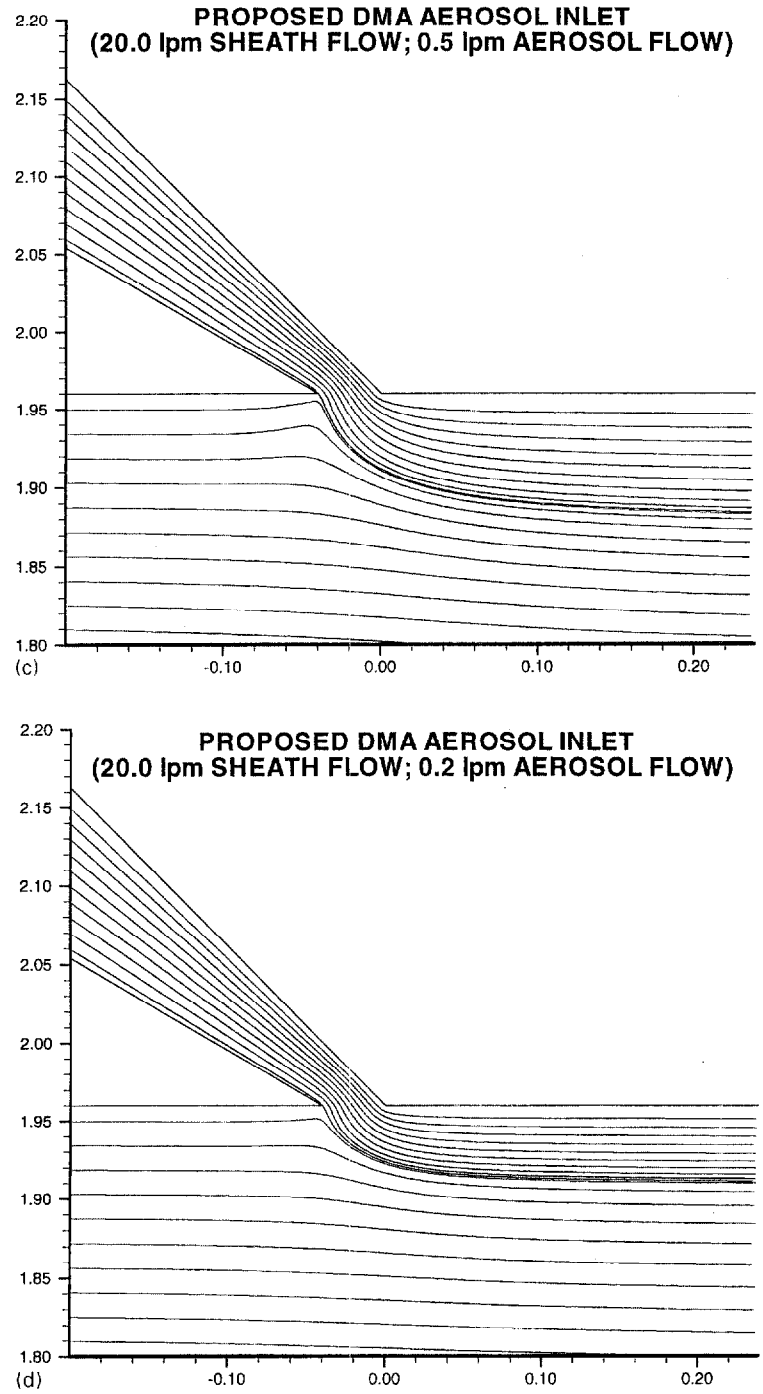

Fig. 8(c) and (d). Flow matching conditions at (c) 8.3 $cm^3 s^{-1}$ (0.5 l min^{-1}) and (d) 3.3 $cm^3 s^{-1}$ (0.2 l min^{-1}) aerosol flow rates when the proposed aerosol entrance slit is installed (The sheath flow is kept constant at 333 $cm^3 s^{-1}$ (20.0 l min^{-1})).

(10 l min^{-1}) of clean, dry air. The aerosol then flowed through a 13 l mixer, which allowed additional time for water evaporation and damping out fluctuations. Next the aerosol flowed through a valve assembly which controlled both the flow and pressure of the aerosol. The aerosol was passed through a bipolar charger and then flowed into DMA 1. The sheath flow rate was set at 333 $cm^3 s^{-1}$ (20 l min^{-1}) and the aerosol flow rate was adjusted to either 33.3, 16.6, 8.3, and 4.2 $cm^3 s^{-1}$ (2.0, 1.0, 0.5, and 0.25 l min^{-1}). The excess air was circulated

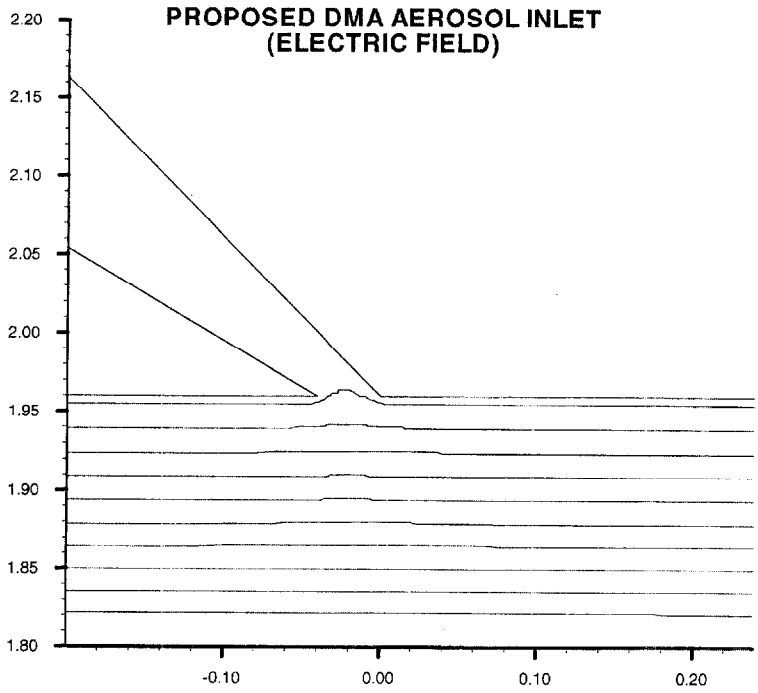

Fig. 9. Electric equipotential lines in the region close to the modified aerosol entrance slit.

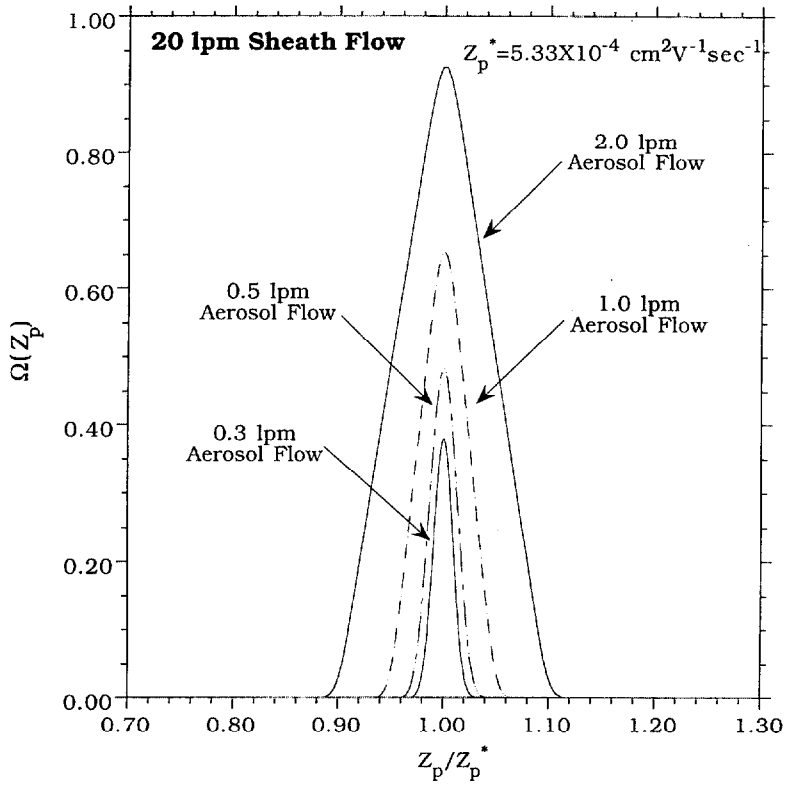

Fig. 10. Numerical transfer function of particles with the central mobility, Z_p^*, of 5.33×10^{-4} cm^2 V^{-1} s^{-1}, at the aerosol flow rates of 33.3, 16.6, 8.3, and 5 cm^3 s^{-1} (2.0, 1.0, 0.5, and 0.3 l min^{-1}) (The sheath flow rate is fixed at 333 cm^3 s^{-1} (20 l min^{-1})).

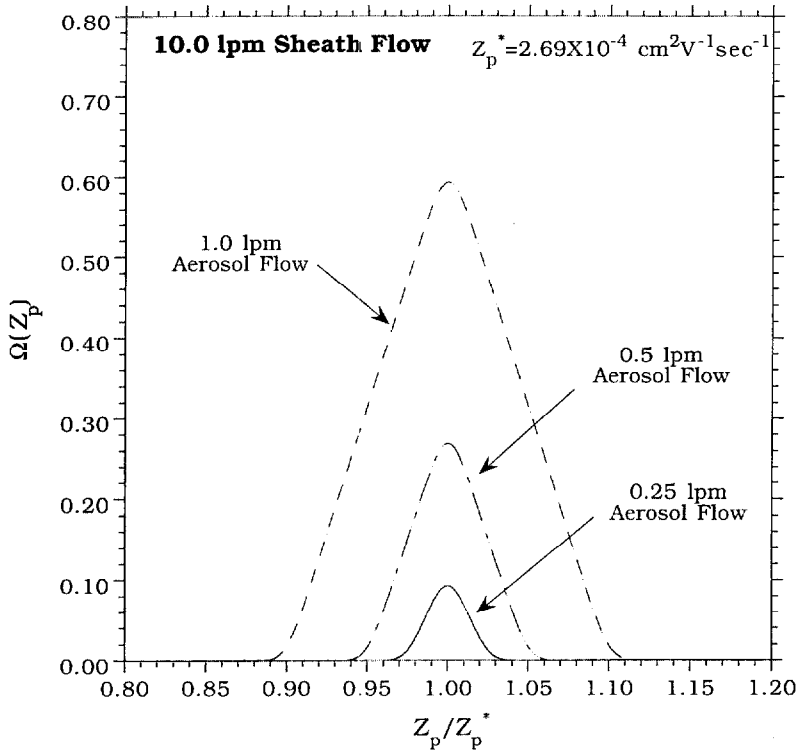

Fig. 11. Numerical transfer function of particles with the central mobility, Z_p^*, of 2.61×10^{-4} cm^2 V^{-1} s^{-1}, at the aerosol flow rates of 16.6, 8.3, 4.2 cm^3 s^{-1} (1, 0.5, and 0.25 l min^{-1}). (The sheath flow rate is fixed at 166 cm^3 s^{-1} (10 l min^{-1})).

back into the inlet for the sheath air, which assured that the sheath and excess flow rates were matched. This was done as described by Mulholland *et al.*(1996) by using two small pumps and buffer tanks before and after the pumps to minimize pulsation, cooling water and an ambient heat exchanger to cool the recirculated air, a filter to remove the particles, silica gel to remove water vapor, and a thermometer to monitor the temperature. The pressure in DMA 1 was monitored at the monodisperse outlet before the valve and was typically about 1.0 kPa above ambient pressure (+10 cm water).

The aerosol exiting DMA 1 entered DMA 2, which was operated in the underpressure mode with the sheath inlet open to ambient pressure. The flow rates were set to match the flows of DMA 1. A typical pressure for DMA 2 was about 2.0 kPa below the ambient pressure (−20 cm water). An automated soap-film flow meter (Gilibrator-2) with calibration flow tubes covering the entire flow range was used for measuring the flow rates. The flow meter was calibrated with the NIST standard flow calibration facility, and the uncertainty at the 95% confidence interval was 1% of the flow rate for a nominal sheath flow rate of 333 cm^3 s^{-1} (20 l min^{-1}).

In determining the flow for the interior of the DMAs, it was important to correct for the pressure difference between the two classifiers. The 3 kPa pressure difference corresponds to a 3% difference in the volumetric flow rates within the classifiers. Electrical mobility of the transmitted particles is directly proportional to the volumetric flow rate so that a 3% larger flow rate corresponds to a 3% increase in the mobility. Therefore, in order to collect particles coming out at the peak voltage of DMA 1 requires a 3% increase in the voltage of the second unit. DMA 1 is always at the higher pressure, so if both DMAs have the same mass flow rate, the peak voltage for the second DMA will always be higher than for the first.

The experimental procedure was to first adjust the sheath flow and monodisperse aerosol flow for DMA 1. The recirculation flow for DMA 1 guaranteed that the sheath flow rate and excess flow rate were matched. When the DMAs are used in tandem, the pressure of the

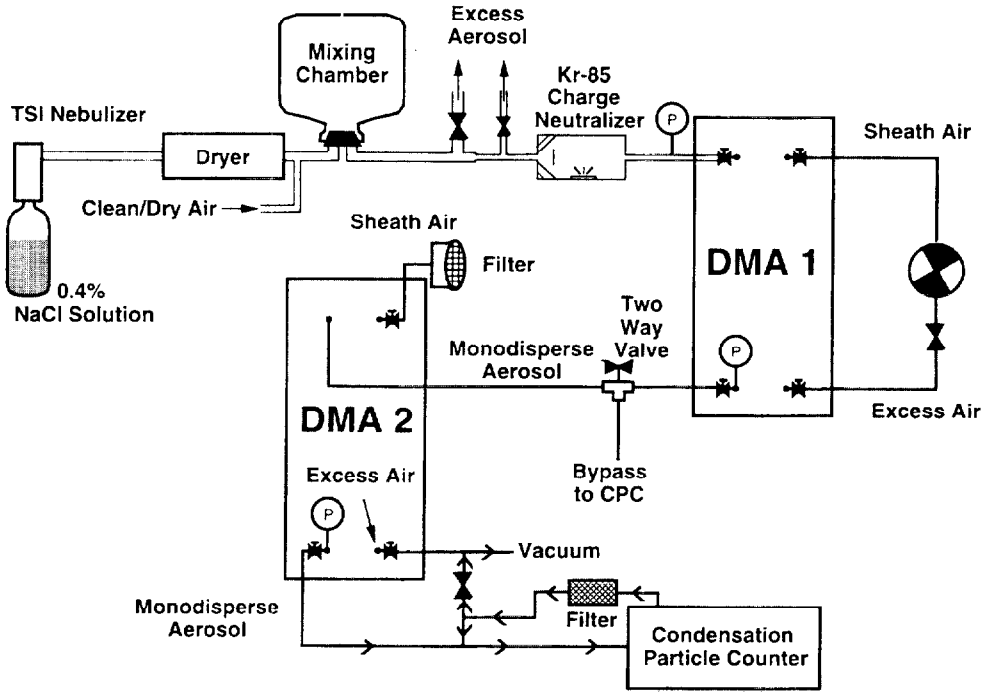

Fig. 12. The schematic diagram of tandem DMA experimental setup.

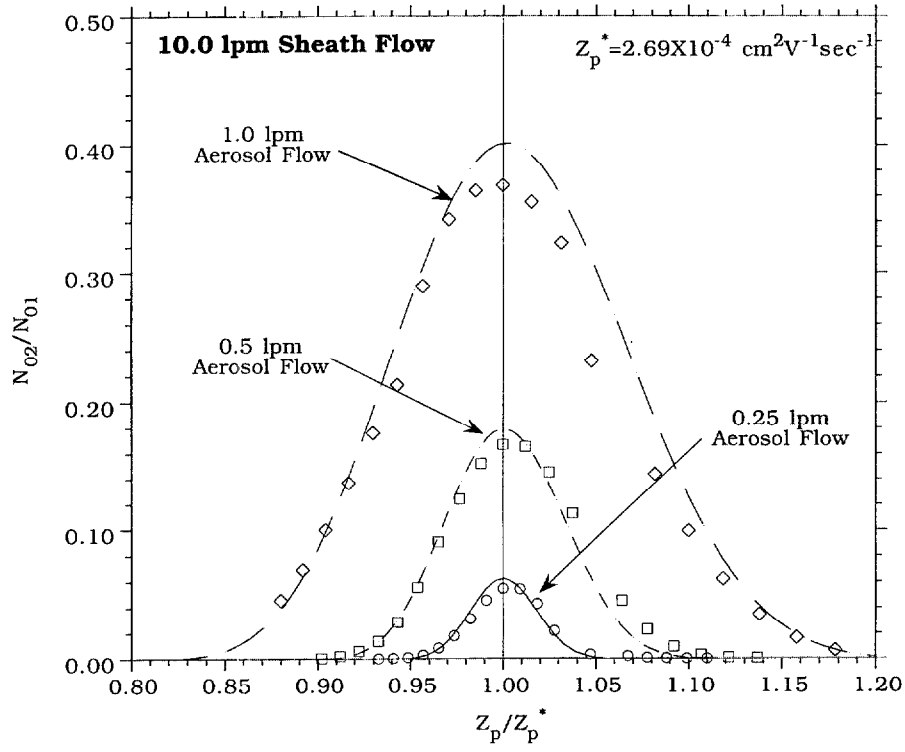

Fig. 13. Comparison of the experimental and numerical TDMA scans at different aerosol flow rates for the case of fixed 166 cm^{3}s^{-1} (10 l min^{-1}) sheath air flow.

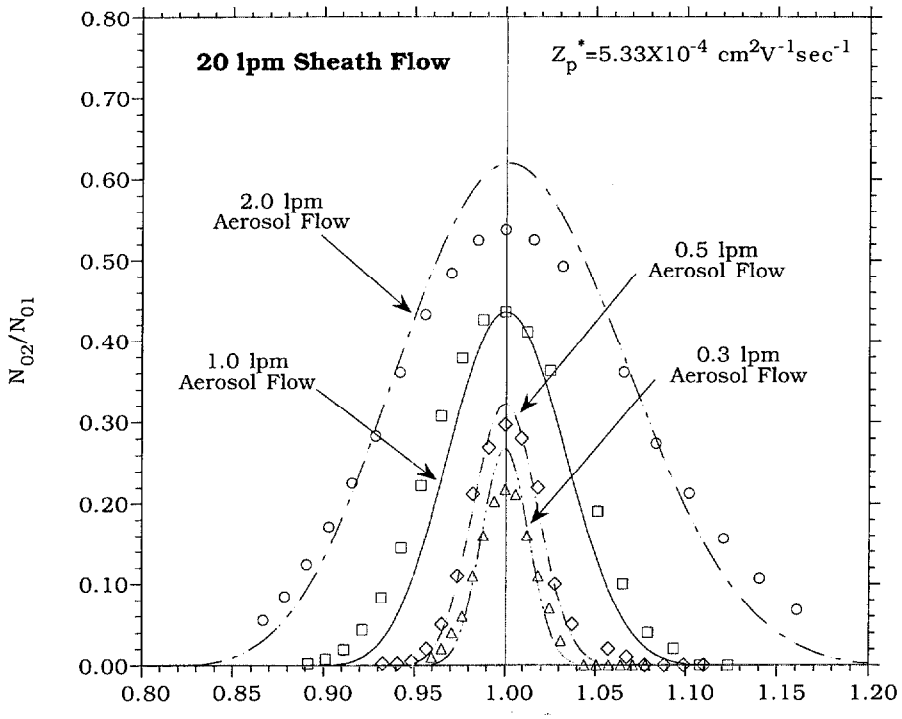

Fig. 14. Comparison of experimental and numerical TDMA scans at different aerosol flow rates for the case of fixed 333 cm^3 s^{-1} (20 l min^{-1}) sheath air flow.

polydisperse aerosol for DMA 2 is reduced to assist in matching both the monodisperse aerosol flow rates as well as the sheath and excess flows in DMA 2. The adjustment of the valve between the vacuum and condensation particle counter (CPC) was critical to obtaining proper flow rates. The adjustments became more challenging as the aerosol flow rate decreases below 1 l min^{-1}.

The data collection of number concentration is computer controlled via the circuitry contained within the CPC (TSI Model 3022A). The number concentration data was recorded for 45 s at each voltage, and data were typically collected at 20 voltage settings with a 40 V difference between successive readings. The data reduction program averaged data over the last 20 s of each voltage to allow the system to fully respond to the change in voltage. Reduced data are plotted as number concentration versus the ratio of the mobility of the DMA 2 to the peak value for DMA 1.

Results and discussion. For the purpose of comparison, numerical TDMA scans are derived from the numerical transfer functions. The scans are convoluted by keeping the numerical transfer function for the first DMA fixed at a central mobility of 1.0 and varying the central mobility of the identical transfer function for the second DMA.

Figure 13 shows comparisons of experimental and numerical TDMA scans at aerosol flow rates of 5, 8.3, 16.6, and 33.3 cm^3 s^{-1} (0.3, 0.5, 1, and 2 l min^{-1}) when the sheath air flow rate is kept constant at 333 cm^3 s^{-1} (20 l min^{-1}). In terms of the width of electric mobility windows, good agreement is obtained at all aerosol flow rates. It should be emphasized that, at an aerosol flow of 5 cm^3 s^{-1} (0.3 l min^{-1}) and a sheath air flow of 333 cm^3 s^{-1} (20 l min^{-1}) the flow ratio is only 1.5%. Thus, we have demonstrated that with the new inlet installed, high resolution measurement using the TSI DMA is possible.

With regards to peak concentration comparisons, the predicted peaks at the smaller aerosol flow rates of 5.0 and 8.3 cm^3 s^{-1} (0.3 and 0.5 l min^{-1}) are higher than those obtained experimentally. This deviation can be explained by particle loss along the exit aerosol transport passage. Small aerosol flows rates give long residence time, resulting in higher

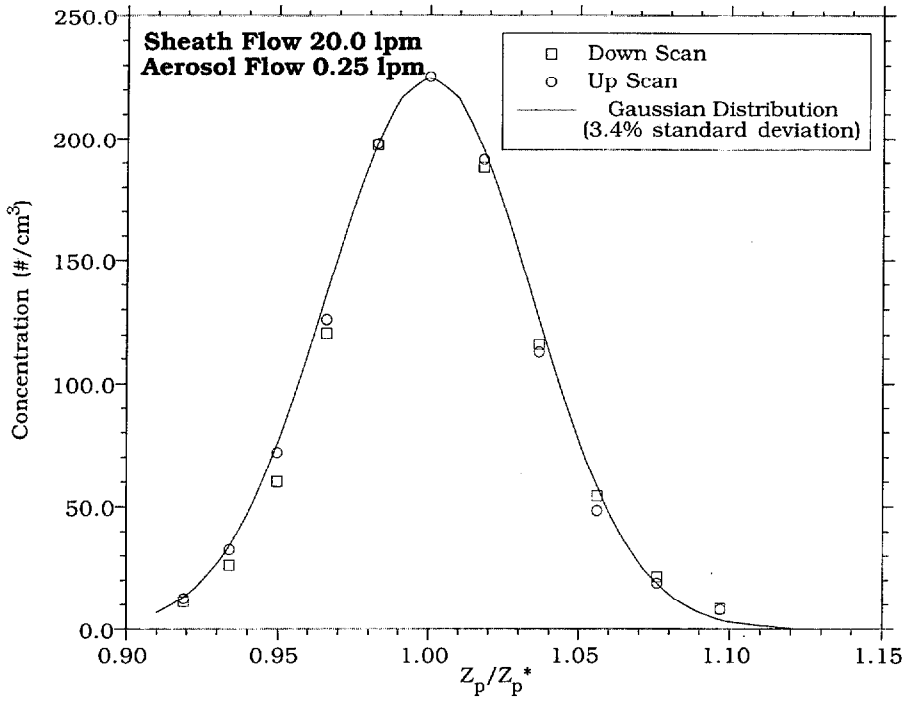

Fig. 15. Results of measuring 0.1 μm SRM using TSI DMA with the improved inlet. The high resolution DMA measurement gives the standard deviation which agrees with the stated values of the SRM.

particle losses in the inlet region. Good agreement is obtained for 16.6 $cm^3 s^{-1}$ (1 l min^{-1}) aerosol flow rate. The agreement is not as good for 33.3 $cm^3 s^{-1}$ (2 l min^{-1}) aerosol flow rate.

A comparison of experimental and numerical TDMA scans at 166 $cm^3 s^{-1}$ (10 l min^{-1}) sheath air flow is shown in Fig. 14. Included in the figure are scans at aerosol flow rates of 4.2, 8.3, and 16.6 $cm^3 s^{-1}$ (0.25, 0.5, and 1.0 l min^{-1}). Good agreement is obtained for 4.2 and 8.3 $cm^3 s^{-1}$ (0.25 and 0.5 l min^{-1}) aerosol flow rates, but agreement is not as good for the 16.6 $cm^3 s^{-1}$ (1.0 l min^{-1}) aerosol flow rate. The smallest flow ratio used in this case is 2.5%. For both the 166 and 333 $cm^3 s^{-1}$ (10 and 20 l min^{-1}) sheath flow cases, the experimental and numerical comparisons for 1/10 flow ratio, i.e. at 16.6 and 33.3 $cm^3 s^{-1}$ (1 and 2 l min^{-1}) aerosol flows, respectively, are not as good as those obtained at the other flow ratios. This implies that flow instability may be the cause of the deteriorating performance. The best operating condition for high resolution measurement using this modified ring appears to be 1/20 flow ratio (1/20, or 0.5/10 aerosol/sheath flows) or lower.

With regards to the problems of voltage shift, it is clearly seen from Figs 13 and 14 that the normalized electric mobilities for each case are symmetrical with respect to the central mobility, i.e. at Z_p/Z_p^* of 1.0. It should be noted that the voltage on the scanned curves shown in the figures was corrected for the pressure difference between the two DMAs. No voltage shift due to the change of the flow ratio is observed. Furthermore, the peak voltage for the second DMA is almost always the same as that applied on the first DMA. The narrow inlet slit appears to be a solution to voltage shift problems. It is also critical that the volumetric flow rates of the two DMAs be matched for there to be no voltage shift.

MEASUREMENT OF 0.1 μm SRM SPHERES USING TSI DMA WITH THE NEW INLET

Figure 15 shows two DMA scans for the 0.1 μm NIST SRM polystyrene spheres. The first scan was obtained by increasing the applied voltage on the TSI DMA from the smallest

voltage setting and the other was by decreasing from the highest voltage setting. In this measurement, the sheath flow rate is set at 333 $cm^3 s^{-1}$ (20 l min^{-1}) and the aerosol flow is 4.2 $cm^3 s^{-1}$ (0.25 l min^{-1}). The flow ratio is 1.5%. The solid line in the figure is curve fit using a Gaussian distribution functional form. The standard deviation obtained is 3.4%. This mobility standard deviation corresponds to a diameter standard deviation of 0.0020 μm, which is the same as the value indicated in the NIST certificate for Standard Reference Material 1963: Nominal 0.1 μm Diameter Polystyrene Spheres. Thus, the improved DMA can measure the standard deviation of SRM particles as well as their mean size.

CONCLUSION

A new inlet for aerosol/sheath flows in the TSI DMA has been designed that makes high resolution measurements attainable The expected performance of the TSI DMA with the new inlet has been evaluated using the numerical model of Chen and Pui (1997). From the numerical results, it was concluded that high resolution measurement could be achieved by reducing the aerosol flow rate while keeping the sheath air flow at a maximum of 333 $cm^3 s^{-1}$ (20 l min^{-1}) or lower flow rates. Calculations indicate that aerosol/sheath flow ratio as low as 0.01 (1%) are feasible. However, the resolution improvement is limited by how low an aerosol flow can be employed. At low aerosol flow, particle losses increase as a result of long residence time in the aerosol inlet.

The tandem DMA technique has been used to verify the performance of the TSI DMA with the improved aerosol inlet. Agreement between the experimental and numerical tandem DMA scans is quite good. This suggests that the improved inlet makes it possible to operate aerosol/sheath flow ratios as low as 1.5%. There is no voltage shift the peak particle concentration in a TDMA configuration operating with the same flow rates in both DMAs. In addition, the voltage shift from reducing the aerosol flow while keeping the sheath air flow rate fixed is no longer observed with the installation of the improved aerosol inlet.

Acknowledgements—We would like to acknowledge the financial support provided by the Microcontamination Research Consortium and the Supercomputer Institute at the University of Minnesota.

REFERENCES

Alonso, A. and Kousaka, Y. (1996) Mobility shift in the differential mobility analyzer due to brownian diffusion and space-charge effects. *J. Aerosol Sci.* **27,** 1201–1225.

Camata, R.P., Flagan, R. C., Vahala, K. J. and Atwater, H. A. (1996) Limits to differential mobility analysis. Presented at *the 15th Annual Conference (AAAR'96)*, 14–18 October, Orlando, Florida.

Chen, D.-R. and Pui, D. Y. H. (1997) Numerical modeling of the performance of differential mobility analyzers for nanometer aerosol measurements. *J. Aerosol Sci.* **28,** 985–1004.

Chen, D. R., Pui, D. Y. H., Hummes, D., Fissan, H., Quant, F. R. and Sem, G. J. (1997) Design and evaluation of a nanometer aerosol differential mobility analyzer (Nano-DMA). *J. Aerosol Sci.* **29,** 497–509.

Kinney, P. D., Pui, D. Y. H., Mulholland, G. W. and Bryner, N. P. (1991) Use of the electrostatic classification method to size 0.1 μm SRM particles—a feasibility study. *J. Res. Nat. Inst. Stand. Technol.* **26,** 147–176.

Knutson, E. O. and Whitby, K. T. (1975) Accurate measurement of aerosol electric mobility moments. *J. Aerosol Sci.* **6,** 453–460.

Kousaka, Y., Okuyama, K., Adachi, M. and Mimura, T. (1986) Effect of Brownian diffusion on electrical classification of ultrafine aerosol particles in differential mobility analyzer. *J. Chem. Engng Jpn.* **19,** 401.

Mulholland, G. W., Bryner, N. P., Liggett, W., Scheer, B. W. and Goodall, R. K. (1996) Selection of calibration particles for scanning surface inspection systems, in flatness, roughness, and discrete defect characterization for computer disks, wafers, and flat panel displays. *Proceedings of the Society of Photo-Optical Instrumentation Engineers*, Vol. 2862, pp. 104–118.

Liu, B. Y. H. and Pui, D. Y. H. (1974) A submicron aerosol standard and the primary, absolute calibration of the condensation nucleus counter. *J. Colloid Interface Sci.* **47,** 155–171.

Rader, D. J. and McMurry, P. H. (1986) Application of the tandem differential mobility analyzer to studies of droplet growth or evaporation. *J. Aerosol Sci.* **17,** 771–787.